Novel lactoferrin-conjugated gallium complex to treat *Pseudomonas aeruginosa* wound infection

Sabeel P. Valappil [a,b,*], Ensanya A. Abou Neel [c,d], Kazi M. Zakir Hossain [e], Willi Paul [f], Durgadas Cherukaraveedu [f], Benjamin Wade [b], Tahera I. Ansari [g], Christopher K. Hope [b], Susan M. Higham [b], Chandra P. Sharma [f]

[a] *Chester Medical School, University of Chester, Bache Hall, Countess View, Chester CH2 1BR, United Kingdom*
[b] *Institute of Population Health, University of Liverpool, Research Wing, Daulby Street, Liverpool L69 3GN, United Kingdom*
[c] *Preventive and Restorative Dentistry Department, College of Dental Medicine, University of Sharjah, Sharjah, United Arab Emirates*
[d] *UCL Eastman Dental Institute, Biomaterials & Tissue Engineering Division, Royal Free Hospital, Rowland Hill Street, London, UK*
[e] *Department of Chemistry, University of Bath, Claverton Down, Bath BA2 7AY, UK.*
[f] *Biomedical Technology Wing, Sree Chitra Tirunal Institute for Medical Sciences and Technology, Thiruvananthapuram 695012, India*
[g] *Northwick Park Institute for Medical Research, Watford Road, Harrow HA1 3UJ, United Kingdom*

ARTICLE INFO

ABSTRACT

Pseudomonas aeruginosa is one of the leading causes of opportunistic infections such as chronic wound infection that could lead to multiple organ failure and death. Gallium (Ga^{3+}) ions are known to inhibit *P. aeruginosa* growth and biofilm formation but require carrier for localized controlled delivery. Lactoferrin (LTf), a two-lobed protein, can deliver Ga^{3+} at sites of infection. This study aimed to develop a Ga-LTf complex for the treatment of wound infection. The characterisation of the Ga-LTf complex was conducted using differential scanning calorimetry (DSC), Infra-Red (FTIR) and Inductive Coupled Plasma Optical Emission Spectrometry (ICP-OES). The antibacterial activity was assessed by agar disc diffusion, liquid broth and biofilm inhibition assays using the colony forming units (CFUs). The healing capacity and biocompatibility were evaluated using a *P. aeruginosa* infected wound in a rat model. DSC analyses showed thermal transition consistent with apo-lactoferrin; FTIR confirmed the complexation of gallium to lactoferrin. ICP-OES confirmed the controlled local delivery of Ga^{3+}. Ga-LTf showed a 0.57 $\log_{10}$ CFUs reduction at 24 h compared with untreated control in planktonic liquid broth assay. Ga-LTf showed the highest antibiofilm activity with a 2.24 $\log_{10}$ CFUs reduction at 24 h. Furthermore, Ga-LTf complex is biocompatible without any adverse effect on brain, kidney, liver and spleen of rats tested in this study. Ga-LTf can be potentially promising novel therapeutic agent to treat pathogenic bacterial infections.

1. Introduction

Pseudomonas aeruginosa is one of the leading causes of opportunistic infections (*e.g.*, wound infection) that can spread systematically through the bloodstream, causing bacteraemia with multiple organ failure and death [1,2]. *P. aeruginosa* bacteraemia among burn patients has accounted for a 28 % increase in mortality [3]. The ability of *P. aeruginosa* to rapidly develop resistance during the course of treating an infection makes this pathogen a priority target for new drug developments [4]. Iron (Fe) metabolism is crucial in the pathogenesis of *P. aeruginosa* infections [5] and has been exploited as a new avenue for antibacterial drug development [6–8]. An estimated 75 % of bacterial

infections involve biofilms, surface-attached colonies of bacteria that are protected by an extracellular matrix [9]. Bacteria protected within biofilms are up to 1000 times more resistant to antibiotics [10] than if they were free-floating (planktonic), and this severely complicates the treatment options. High levels of Fe^{3+} are required for the formation of cell clusters early in the biofilm development and for the maturation of biofilms into three-dimensional structures [11]. The fact that the host defences severely limit the available Fe and the importance of Fe in infection suggest that invading organisms may be vulnerable to interventions that further disrupt Fe acquisition or metabolism [6].

It was reported that gallium (Ga^{3+}) ions inhibit *P. aeruginosa* growth and biofilm formation *in vitro* by decreasing bacterial Fe^{3+} uptake and

interfere with iron signalling *via* the transcriptional regulator *pvd*S [6]. Gallium has already been approved by the FDA to treat hypercalcaemia of malignancy [12] and has recently emerged as a new generation antibacterial ion that may be useful in treating and preventing localized infections [6]. Gallium is known to possess chemical properties that are similar to those of Fe^{3+} such as ionic radius, coordination chemistry and ionisation potential. Gallium might therefore act as a 'Trojan horse' by exploiting the inability of biological systems to distinguish Ga^{3+} from Fe^{3+} [13]. Additionally, Ga^{3+} can block Fe^{3+}- dependent processes because unlike Fe^{3+}, Ga^{3+} cannot be reduced under the same conditions but sequential oxidation and reduction are essential for many of the biological functions of Fe^{3+} and crucial energy metabolism of bacteria [13]. Ga^{3+} is not integrated in haem and so does not result in human cell cytotoxicity resulting from the interruption with oxygen transport and cytochrome mediated reactions [14]. Furthermore, due to its active metabolism and rapid growth, bacteria are favoured targets for Ga^{3+} action [15]. Therefore, local delivery of Ga^{3+} at the site of infection may boost its antibacterial action while being less toxic to host cells. Research in this area focuses on the exploitation of Ga^{3+} delivery from different complexes, including gallium maltolate [16], desferrioxamine gallium [17], gallium salts (*e.g.* $Ga(NO_3)_3$) [18], gallium carboxymethyl cellulose, [19,20] gallium alginate, gallium pectin, gallium doped phosphate based glasses [8] and gallium curcumin [21]. However, the therapeutic use of Ga^{3+} for treatments such as wound infections requires advancements in effective local delivery and its bioavailability. From this perspective, lactoferrin which is a two-lobed protein with a molecular weight of approximately 80,000, can bind two Fe^{3+} or Ga^{3+} ions and deliver these ions at sites of infection [22]. Therefore, lactoferrin seems to be a promising candidate. Furthermore, lactoferrin is abundant in many epithelial secretions such as milk, tears, nasal secretions and seminal fluid; it is normally present in amounts of 0.5 to 1 mg/mL [23]. It is also found to be concentrated at sites of inflammation and infection, mainly in granulomatous neutrophils and polymorphonuclear leukocytes [24,25]. Extracellular lactoferrin at such sites is derived primarily from pathogen stimulated neutrophils [26,27]. If Ga^{3+} is conjugated with lactoferrin, the local production of bacterial and neutrophil proteases and the low pH could facilitate Ga^{3+} release from lactoferrin leading to a significant level of free antibacterial Ga^{3+} at the site of infection.

The aim of this study was therefore to develop novel gallium conjugated lactoferrin complex and evaluate their antibacterial activity against *Pseudomonas aeruginosa* ATCC 27853 in both *in vitro* and as *in vivo* rat wound infection models. The objectives of this study are: (a) preparation and characterisation of Ga-LTf using DSc, FTIR, and SEM-EDS, (b) detection of gallium ion release using ICP-OES, (c) testing the antibacterial action of Ga-LTf against *P. aeruginosa* using disc diffusion, liquid broth and biofilm assays, (d) characterisation of *P. aeruginosa* biofilm using Raman mapping, (e) testing the *in vivo* biocompatibility and antibacterial efficacy of Ga-LTf using male Sprague Dawley rats.

2. Experimental procedures

2.1. Preparation of Ga-LTf complex

A lactoferrin (L0520 Sigma Aldrich, Lot number SLBB2642V, Dorset, UK) solution was prepared in deionised water at a concentration of 1 mg/mL. Then to 5 mL of lactoferrin solution, 5 mL of 0.2 mM gallium chloride solution (99.99 %, Sigma Aldrich, Dorset, UK) was added drop wise by stirring using a magnetic stirrer at 10 °C. After 5 min, a drop of 0.1 M NaOH was added to adjust the pH to 10. Then 100 μL of 0.1 mM sodium borohydride (99.99 %, Sigma Aldrich, Dorset, UK) was added to reduce the gallium chloride and the reaction was continued for 6 h at 10 °C for the formation of Ga-LTf complex. Dialysis of the suspension was then performed for 12–24 h in deionised water to remove the excess sodium hydroxide.

2.2. Physico-chemical characterisation of Ga-LTf complex

2.2.1. Differential scanning calorimetry (DSC)

The thermal behaviour of LTf and Ga-LTf was carried out using a differential scanning calorimetry (TA Q20 Instrument, Waters LLC, New Castle, UK) under nitrogen atmosphere after being calibrated using zinc and indium as standards. Samples ($n = 3$) of 5 mg were sealed in aluminium pans and heated from 0 to 200 °C at 10 °C/min.

2.2.2. Fourier transform infrared spectroscopy (FTIR)

The chemical functional groups of the LTf and Ga-LTf were identified at room temperature using an FTIR spectroscopy (Tensor-27, Bruker, Germany) equipped with a standard attenuated total reflectance (ATR) cell (Pike Technology, UK). Samples were scanned in transmittance mode over the wavenumber range from 4000 to 550 cm^{-1} and at a resolution of 1 cm^{-1}.

2.2.3. Inductively coupled plasma optical emission spectrometry (ICP-OES)

Approximately 1 mL of Ga-LTf complex was incubated in 5 mL of phosphate buffer saline (PBS, Oxoid Ltd., Basingstoke, UK) at 37 °C for 48 h in a sealed dialysis tube. The Ga^{3+} ion release from the Ga-LTf complex was investigated at different time points (6, 12, 24, 36 and 48 h) using inductively coupled plasma optical emission spectrometry (ICP-OES spectrometer, Optima 5300, Perkin Elmer, USA) after being calibrated for the predicted concentration range using gallium nitrate (Sigma Aldrich, Dorset, UK) solutions as standards. The samples and standards were digested in high purity nitric acid; the emission was recorded at 294.364 nm and analyzed using WinLab 32 software. The data were reported as amount of Ga^{3+} ion release (ppm) as a function of time (h).

2.2.4. Scanning electron microscopy (SEM)-electron dispersive X-ray spectroscopy (EDS)

The morphology of the LTf (as received) and freeze-dried Ga-LTf samples were studied using scanning electron microscopy (SEM, Hitachi SU3900) at an accelerating voltage of 20 kV. Elemental analysis was performed using SEM-EDS integrated system utilising an Ultim Max 170 detector (Oxford Instruments). Standards used for chemical composition analyses were pure element (for C), BN (for N and B), SiO_2 (for O), albite (for Na), gallium phosphide (for Ga), NaCl (for Cl), and FeS_2 (for S).

2.3. Antibacterial analyses of Ga-LTf complex

2.3.1. Disc diffusion assay

The ability of Ga-LTf complex to inhibit the growth of *P. aeruginosa* was investigated using the disc diffusion method [28]. Freshly prepared Iso-sensitest (IST, Oxoid Ltd., Basingstoke, UK) agar plates were inoculated with standardized cultures of *P. aeruginosa* (approx. 10^8 cells/mL). One hundred microliters of Ga-LTf complex solution (gallium concentration 2 μg/100 μL) were added on the *P. aeruginosa* inoculated IST agar plates as the experimental samples. One hundred microliters of LTf solution were first loaded on to blank disc cartridges (Oxoid Ltd., Basingstoke, UK) and used as a negative control. Furthermore, 10 μg tobramycin discs (Oxoid Ltd., Basingstoke, UK) were placed on the *P. aeruginosa* inoculated IST agar plates and used as a positive control. All IST agar plates were incubated aerobically at 37 °C for 48 h. The diameters of any zone formed around the discs were measured in millimetres using callipers and compared with both controls. All experiments were conducted in triplicate.

2.3.2. Liquid broth assay

A loop full of *P. aeruginosa* grown on IST agar was inoculated into 10 mL of IST broth and incubated overnight at 37 °C with 200 rpm agitation in an Orbital Shaker (Stuart Scientific, UK). The overnight cultures were used to inoculate 5 mL of phosphate buffer saline (PBS) (Oxoid Ltd., Basingstoke, UK) to a standardized optical density of 0.03 at a

wavelength of 600 nm (OD$_{600}$). Then 200 μl of 8 mg/L tobramycin (positive control), 200 μl of LTf (negative control) or 200 μl of test sample (Ga-LTf) was added to each tube as appropriate. The tubes were then incubated at 37 °C. At various time intervals (2, 4, 6 and 24 h), serial dilutions of the suspensions were carried out in PBS. Then 10 μl of the suspension and each dilution was spread onto on brain heart infusion agar (BHI, Oxoid Ltd., Basingstoke, UK) plates. The plates were then incubated aerobically at 37 °C for 48 h. For each type of disc, viable counts (colony forming units; CFUs) were conducted in triplicate.

2.3.3. Biofilm assay

A Constant-Depth Film Fermenter (CDFF) was used for the production of *P. aeruginosa* biofilms [8,29]. The CDFF has a stainless-steel turntable and 15 polytetrafluoroethylene (PTFE) pans; each pan has 5 PTFE plugs. In each PTFE pan, 5 mm diameter hydroxyapatite (HA) disc, that supports the biofilm growth, was loaded on each plug and recessed by 200 μm. The pans were then flushed with the turntable. A cylindrical glass vessel, top and bottom steel plates enclosed the turntable. The top plate contained an air inlet port attached to two 0.2 μm high-efficiency particulate air filters (Thermo Fisher Scientific, Loughborough, UK) and three medium inlet ports. Prior to the experiment, the CDFF was sterilized in a hot air oven at 140 °C for 3 h. For this experiment, 10 mL of 24-h *P. aeruginosa* culture inoculated into 0.5 L of 40 % tryptic soy broth (TSB, Oxoid Ltd., Basingstoke, UK) was used. After 6 h, the fermenter was fed from an 8-L medium reservoir of 40 % TSB at 0.5 mL/min using a peristaltic pump (Watson and Marlow, Falmouth, UK). The TSB was distributed over the pans by two scraper blades that maintain the required depth of biofilms on the discs. The bottom plate contained a medium outlet port to drain effluent. Throughout the experiment, the CDFF was incubated at 37 °C and rotated at 3 rpm. At various time intervals (6, 24, 48 and 120 h), the pans were removed aseptically, and biofilm grown on HA discs were immersed into either 200 μLof 8 mg/L tobramycin (positive control), 200 μL of ultrapure water (negative control) or 200 μL of Ga-LTf with a gallium concentration of 2 μg/100 μL (test sample). After 10-min exposure, the specimens were rinsed three times with 20 mL of sterile ultrapure protease free water (Sigma-Aldrich, Dorset, UK) to remove any active compounds. The discs were then transferred to separate containers, having sterile glass beads and 5 mL of sterile distilled water, and vortexed for 1 min to remove and disperse the attached biofilm into suspension. For each specimen, serial dilutions of the suspensions were carried out in PBS; 10 μL aliquots of the diluted suspensions was spread onto BHI plates and incubated aerobically at 37 °C for 48 h. Then for each treatment, the CFUs were counted in triplicate and presented as log$_{10}$ values as a function of time.

2.3.4. Raman mapping of P. aeruginosa biofilm

Confocal Raman microscope (Witec Inc. alpha300R) was used to study *P. aeruginosa* biofilm on HA substrate as well those treated with Ga-LTf and tobramycin. Raman mapping was carried out using frequency-doubled Nd-YAG laser with 532 nm, SP2300i spectrometer and back illuminated Peltier cooled CCD camera DU401A. A x50 Nikon objective lens (NA = 1.0) was used to collect Stokes shifted Raman spectra in 400–4000 cm^{-1} range and 1 cm^{-1} resolution. 2D array of Raman spectral images was recorded every 0.5 s at a scan depth of 80 × 80 points for 150 × 200 μm^2. The distribution of Raman spectra over the examined cell were colour coded to differentiate between biofilm and the HA substrate background.

2.4. In vivo biocompatibility and antibacterial efficacy of Ga-LTf complex

All animal experimentation including surgery and husbandry was conducted in accordance with the Animal (Scientific) Procedures Act 1986 and Home Office code of Practice and it was carried out under project licence PPL 80/2200. The *in vivo* antibacterial action of Ga-LTf complex was performed on an artificially induced *P. aeruginosa* wound infection model. The study was performed on male Sprague Dawley rats,

weighing approximately 300 g. In total, 9 rats were used to evaluate the effect of Ga-LTf (*n* = 3), tobramycin (n = 3) and sterile distilled water (n = 3) as negative control. Wounds were created in the animals and infection induced with 3/0 Mersilk® sutures (Ethicon, Johnson & Johnson Medical Ltd., UK) contaminated with *P. aeruginosa* at 2.0×10^9 cells/mL. The wounds were then treated twice daily with 200 μL Ga-LTf (gallium concentration 2 μg/100 μL), tobramycin (8 mg/L) or sterile distilled water. The total number of *P. aeruginosa* from the wound at the end of the 7 days' experiment was assessed using the wound washing method [30]. Pseudomonas selective agar was used for plating serial dilutions of the wound wash lavage. These plates were incubated at 30 °C for three days to enumerate the CFUs of *P. aeruginosa*.

Photographs of the wound healing process were taken at the beginning, 3rd and 7th day. The internal organs (kidney, liver, spleen, and brain) were taken after the animals' termination and processed for histological analyses for the systemic involvement of *P. aeruginosa*. Specimens of all organs were fixed in 10 % neutral buffered formal saline (Genta Medical, UK) for a minimum of 24 h. Tissues were processed by routine automated procedures to wax embedding. Sections of 5 μm were cut from each block and stained with Haematoxylin & Eosin and Picro-sirius red with Miller's elastin for histological analysis.

2.5. Statistical analysis

Data analyses were performed in Excel (Office 365 Version 1901: Microsoft Corporation, Redmond, WA, USA). One-way analysis of variance (ANOVA) was used to compare mean viable counts, following arcsine transformation of data. When a significant difference was detected, a Tukey test was conducted to find which values were different (GraphPad Software; 162 San Diego, USA.) Statistical significance was defined at a level of $P < 0.05$.

3. Results

Fig. 1(a) shows the diagrammatic representation of Ga-LTf formation that was prepared following a conventional reduction complexation approach at pH of 10. The lactoferrin is a simple polypeptide chain folded into two symmetrical, homologous N and C lobes with two Ga^{3+} binding sites. LTf is a basic protein and has a high propensity to interact with negatively charged molecules in thesolution [31]. LTf used in this study has an isoelectric point (pI) of 8.7, iron saturation of 4.7 % and molecular weight of 82.4 kDa (provided by the certificate of analysis of lactoferrin from the supplier) suggesting a high degree of glycosylation [32] that might enhance its adsorption onto dialysis tube surfaces and potential change in the conformation of Ga-LTf. It is proposed that the Phosphate buffer saline environment (pH 7.3 at 37 °C) could have promoted cation exchange, leading to the incorporation of Na or K on specific Ga-LTf sites, resulting in leaching of Ga^{3+} presumably as GaCl$_3$.

3.1. Physico-chemical characterisation of Ga-LTf complex

3.1.1. Differential scanning calorimetry (DSC)

Fig. 1(b) shows the DSC thermogram of LTf and Ga-LTf complex. Lactoferrin shows a transition at 75.33 °C. The complexation of Ga with lactoferrin shifted the transition peak to a higher temperature (90.26 °C); this was also associated with the appearance of another peak at 180.23 °C.

3.1.2. Fourier transform infrared spectroscopy (FTIR)

Fig. 1(c) shows the functional groups of the LTf and Ga-LTf complex that were identified using FTIR analysis. Pure LTf exhibited a characteristic broad band around 3100–3650 cm^{-1} with the highest peak at 3278 cm^{-1} which was attributed to -NH$_2$ (amide A band of protein) and –OH stretching vibrations. The characteristic peaks at 2961 and 2872 cm^{-1} are associated with the bands of antisymmetric CH$_2$ stretching and symmetric CH$_2$ stretching, respectively. The bands at 1638 and 1522
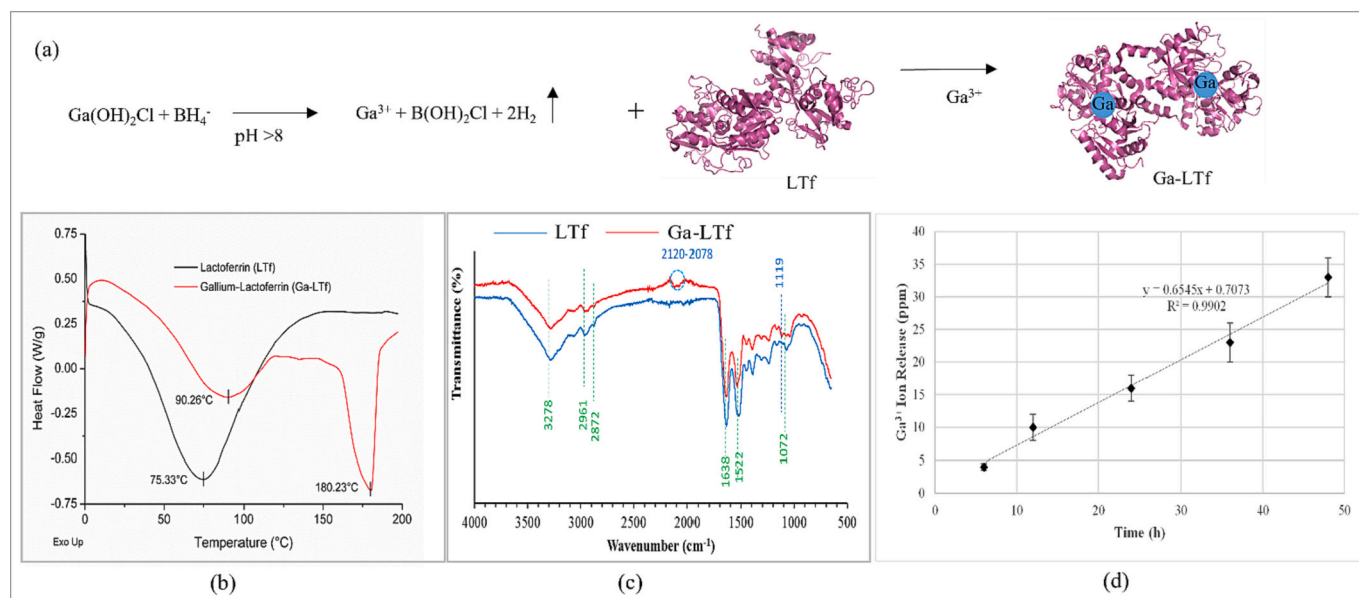
Fig. 1. Schematic representation of (a) possible Ga^{3+} ions formation and complexation with LTf (PDB code = 1CB6) to form the Ga-LTf (based on PDB code = 1B0L, blue spheres represent Ga^{3+} binding sites) and (b) DSC thermogram of LTf and Ga-LTf showing a second transition and complexation. (c) FTIR spectra of LTf and Ga-LTf showing gallium complexation with LTf. (d) The Ga^{3+} release in ppm from Ga-LTf stored in phosphate buffer saline as a function of time.

cm^{-1} are assigned to C=O stretching vibration of amide I and N—H and C—H bending vibration absorption of amide II of protein, respectively [33]. The band at 1067 cm^{-1} is assigned to the N≡C or C=C stretch and C—H deformation vibrations [34].

In the case of Ga-LTf complex, all the functional groups of the pure LTf are seen to be present without any noticeable shifting of the major bands. However, the bands at 2020–2070 cm^{-1} and 1119 cm^{-1} are suggested to be due to the Ga—H bond [35] and B—H bending vibration [36,37] respectively, which were originated from the use of $GaCl_3$ and $NaBH_4$ during the Ga-LTf complex formation.

3.1.3. Inductively coupled plasma optical emission spectrometry (ICP-OES)

Fig. 1 (d) shows Ga^{3+} ion release from Ga-LTf complex incubated in phosphate buffer saline over a period of 48 h. As observed, Ga^{3+} ion release increased linearly with time; the release rate, denoted by the slop of the linear fit, is 0.6545 ppm/h. During the first 6 h, the amount of Ga^{3+} ion release was 4 ± 0.5 ppm; the release of Ga^{3+} ions increased by one order of magnitude at 48 h to reach to 33 ± 3 ppm.

3.1.4. Scanning electron microscopy (sem)-electron dispersive X-ray spectroscopy (EDS)

Fig. 2 shows the SEM of the as-received pure LTf and Ga-LTf complex. The as-received LTf shows flake-like morphology, as can be seen in Fig. 2 (I). The elemental composition of the LTf are shown in Table 1, and the elemental mapping [Fig. 2 (I)] shows the presence of the C, N, O and S group in the pure LTf. After complex formation with $GaCl_3$ and $NaBH_4$, the Ga-LTf complex also showed flake-like morphology, similar to the pure LTf. Apart from the main elements (C, N, O and S) of the LTf, additional Na, Cl, Ga and B elements were found-Table 1 and Fig. 2 (II). This was expected as $GaCl_3$ and $NaBH_4$ were used in the complex formation reaction. These elements are also seen in the EDS mapping images.

3.2. Antibacterial analyses of Ga-LTf complex

3.2.1. Disc diffusion assay

Planktonic growth inhibitory assay performed on *P. aeruginosa* to establish the antibacterial action of Ga-LTf complex -Fig. 3(a). The zones of inhibition (*i.e.* zones of no visible bacterial growth surrounding the

material) were found to be 14.5 ± 0.5 mm for Ga-LTf compared with 25 ± 0.5 mm for tobramycin and 1 ± 0.5 mm for lactoferrin.

3.2.2. Liquid broth assay

The antibacterial effects of Ga-LTf complex on planktonic growth of *P. aeruginosa* were also evaluated in liquid medium, PBS. Fig. 3(b) shows the antibacterial action of Ga-LTf in comparison to lactoferrin, tobramycin (as a positive control) and untreated (as a negative control). Initial viable counts were conducted prior to the addition of the test agents to check the viability of the bacteria. Both Ga-LTf and tobramycin showed a statistically significant ($p \leq 0.05$) reduction in the log_{10} of the mean number of viable cells until 24 h. However, there was no statistically significant ($p > 0.05$) difference between log_{10} of the mean number of viable cells of untreated and LTf treated samples throughout the experiment. The antibacterial effect was more pronounced in samples treated with tobramycin, with a maximum effect of 1.72 log_{10} CFUs reduction compared with untreated samples at 24 h. With Ga-LTf, a maximum effect of 0.57 log_{10} reduction in CFUs compared with untreated samples at 24 h.

3.2.3. Biofilm assay

The anti-biofilm activity of Ga-LTf complex was evaluated on *P. aeruginosa* biofilm grown in a CDFF [8] using HA substrates. Fig. 3(c) shows the anti-biofilm activity of Ga-LTf in comparison to tobramycin as positive control and water as negative control. Biofilm samples that were extracted after 6 h of incubation and exposed to Ga-LTf complex and tobramycin showed a statistically significant difference in log_{10} of the mean number of viable cells compared with the negative control, water ($p \leq 0.0006$). But, Ga-LTf complex showed no statistically significant difference ($p = 0.09$) from tobramycin at 6 h. At 24 h, the log_{10} of the mean number of viable cells was significantly reduced for both Ga-LTf complex and tobramycin compared with water ($p = 0.0001$). But again at 24 h, there was no significant difference ($p = 0.086$) between Ga-LTf complex and tobramycin. The anti-biofilm effect of Ga-LTf complex and tobramycin was statistically significant ($p \leq 0.001$) when compared with water at 48 h, but the effect of Ga-LTf was found to be less when compared with that of tobramycin. The greatest effect of Ga-LTf on biofilm growth was observed at 24 h (2.24 log_{10} CFUs reduction compared with water), whereas for tobramycin this was seen at 120 h
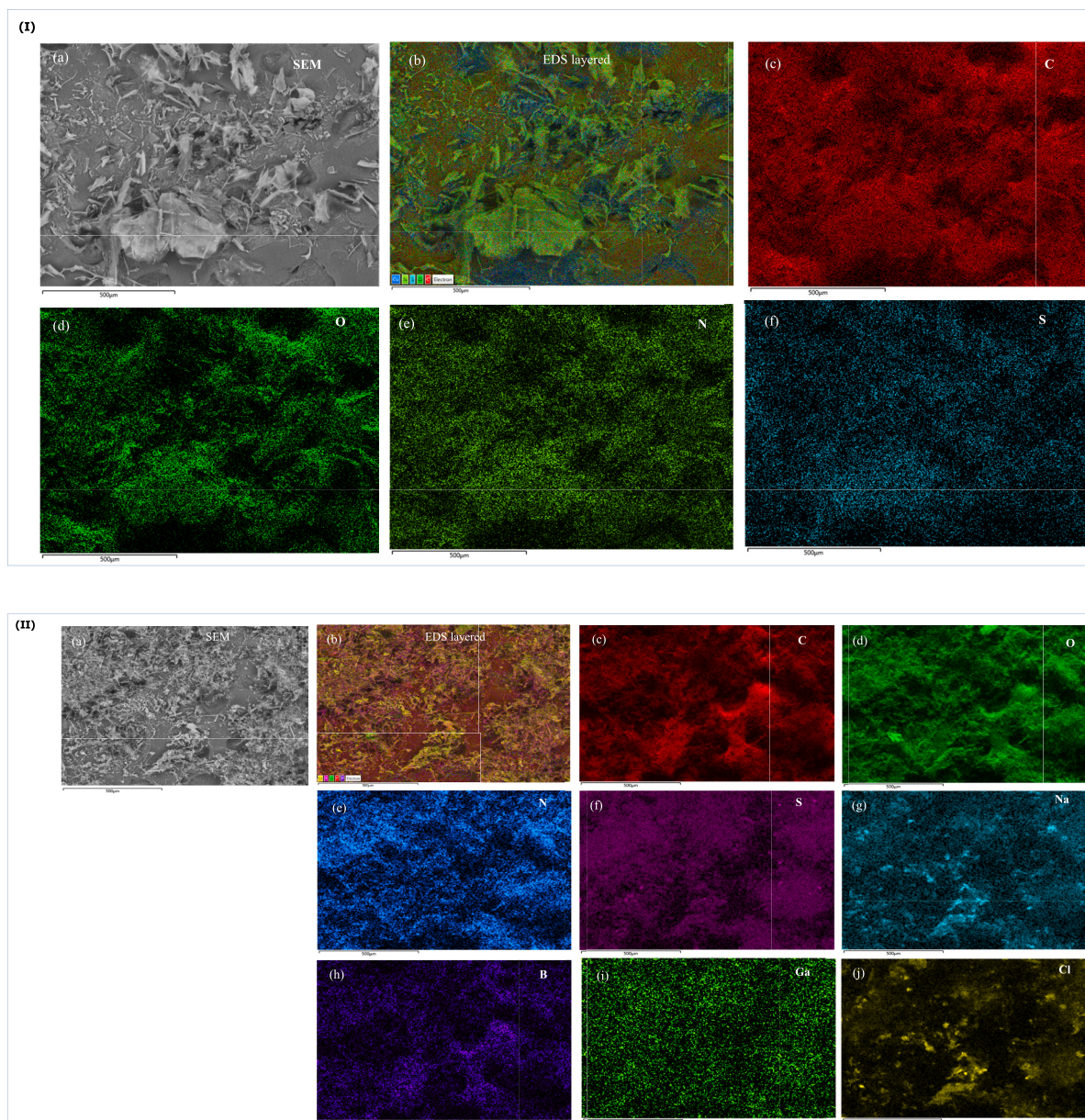
Fig. 2. (I) SEM (a) and elemental mapping of C, O, N and S of as-received pure LIf (b-i respectively. II SEM (a) and elemental mapping of C, O, N, S, Na, B, Ga and Cl of Ga-LTf.

Table 1
Elemental compositions of LTf and Ga-LTf complex.

Element	LTf (wt%)	Ga-LTf (wt%)
C	53.78	52.63
N	17.18	17.21
O	26.09	25.44
S	2.95	2.35
Na	–	0.61
Cl	–	0.87
Ga	–	0.59
B	–	0.30

(4.32 $\log_{10}$ CFUs reduction compared with water). However, at 120 h the $\log_{10}$ of the mean number of viable cells on Ga-LTf started to recover from the previous low number at 48 h and showed no statistically significant difference ($p = 0.11$) compared with water, but tobramycin still showed a statistically significant difference compared with water ($p =$

0.001).

3.2.4. Raman mapping of P. aeruginosa biofilm on HA substrate

Fig. 3(d) shows the Raman mapping of *P. aeruginosa* biofilm grown on HA substrate and treated with Ga-LTf in comparison to tobramycin-treated (positive control) and untreated samples (negative control). The distribution of the Raman spectra over the examined Raman Shift Cell were colour-coded and clearly differentiated between the *P. aeruginosa* biofilm and the HA substrate. Fig. 3(d) shows a cross-sectional image in the x-z orientation of a biofilm assembled from 2800 to 3050 cm^{-1} peaks showing the distribution of all organic components which corresponds to the biofilm (red), 920–970 cm^{-1} peaks representing the hydroxyapatite substrate on which the biofilm was grown (blue) and region corresponds to air (navy blue). As observed, the biofilm on HA substrate which received no treatment was the thickest (~100 μm) compared with tobramycin- and Ga-LTf-treated samples. Additionally, Ga-LTf-treated biofilm thickness (~20 μm) was less compared with that of tobramycin treated biofilm (~25 μm).
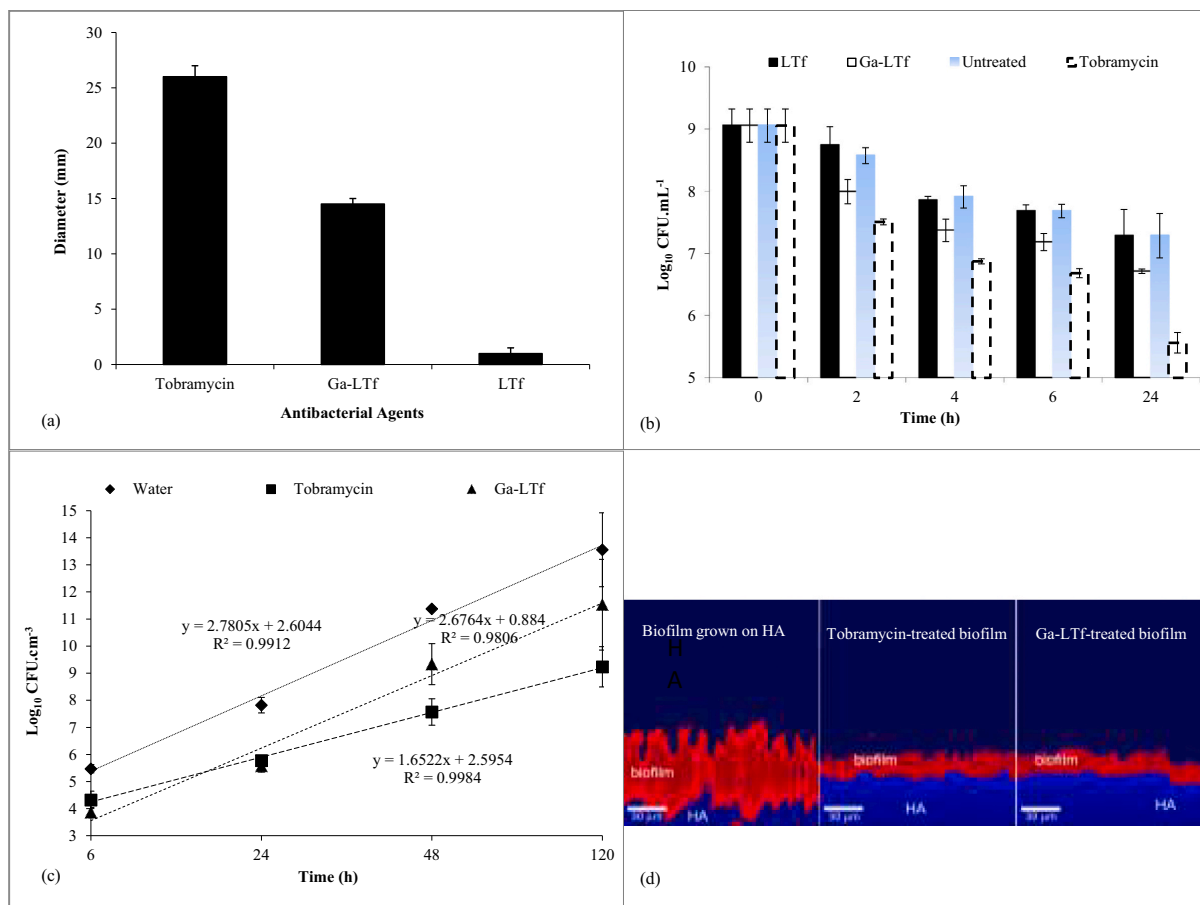
Fig. 3. (a) Agar diffusion assay showing the inhibition zone of *P. aeruginosa* treated with Ga-LTf complex in comparison to tobramycin and lactoferrin. (b) Liquid broth assay showing the viability *P. aeruginosa* suspension, indicated by $\log_{10}$ CFUs, after 2, 4, 6 and 24 h incubation with Ga-LTf complex in comparison to tobramycin, lactoferrin and untreated control. (c) Biofilms assay showing the $\log_{10}$ CFUs of *P. aeruginosa* grown on HA and exposed for 10 min to Ga-LTf, tobramycin or water as a function of time. Error bars represent standard deviation (SD) from the mean. (d) Raman mapping of biofilm grown on HA (control) in comparison to tobramycin-treated or Ga-LTf-treated biofilm. Biofilm (red), HA (light blue- bottom), and air (dark blue- top).

3.3. In vivo biocompatibility and antibacterial efficacy of Ga-LTf complex

Biocompatibility and the *in vivo* antimicrobial effects of Ga-LTf composites were performed on an artificially induced *P. aeruginosa* wound infection healing study. Fig. 4 shows the healing process of the infected wound at different time points after being treated twice daily with 200 μL Ga-LTf (gallium concentration of 2 μg/100 μL) in comparison to tobramycin-treated (8 mg/L, positive control) and sterile distilled water-treated wounds (negative control). As observed, the healing was faster as indicated by the reduction in wound size in Ga-LTf-treated group followed by tobramycin-treated and then water treated group. Furthermore, the total number of *P. aeruginosa* recovered from the wound, by the wound washing method [30], at the end of the 7-day experiment was assessed using Pseudomonas selective agar plates. The results showed that there was no significant difference in the number of CFUs between samples collected from tobramycin-, Ga-LTf-treated or water-treated animals.

Fig. 5 shows the histological sections of the kidney, brain, liver and spleen of the terminated rats to analyse the systemic involvement of *P. aeruginosa*. As observed, there was no significant difference in any of the internal organs with regards to cellular morphology in rats treated with Ga-LTf, water or tobramycin. This finding suggests that there was no systemic involvement of *P. aeruginosa* infection in any of the animals tested. Furthermore, there was no evidence of any sign of inflammation in any of the tested groups.

4. Discussion

This paper reports on the production of a novel complex of lactoferrin conjugated gallium, its physico-chemical characterisation, antibacterial/antibiofilm effect on *P. aeruginosa in vitro* and *in vivo* rat wound infection model. Ga-LTf was prepared following a conventional reduction complexation approach. Coordination chemistries of Ga^{3+} and Fe^{3+} are very similar except that Ga^{3+} is irreducible at physiological pH [13]. Therefore, Ga-LTf complex was prepared in a medium with a pH of 10. Like transferrin, lactoferrin is a simple polypeptide chain folded into two symmetrical, highly homologous (N and C) lobes that have two Ga^{3+} binding sites (interdomain cleft of each lobe). Unlike transferrin, lactoferrin binds gallium more strongly by a factor of ~90 [38].

The endothermic peak, appeared in DSC thermogram at 75.33 °C, is consistent with apo-lactoferrin as confirmed by the certificate of analysis of lactoferrin from the supplier (L0520 Sigma-Aldrich, Lot number SLBB2642V, Dorset, UK). As revealed by the supplier, the lactoferrin has only trace amounts of Fe^{3+} (79 ppm) [37]. Ga-LTf shows a double transition with the first peak shifting towards 90.26 °C due to the gallium saturation of lactoferrin [39] which confirms gallium complexation with lactoferrin.

Ga-LTf complex was prepared by simple addition of dilute lactoferrin solution to $GaCl_3$ in the presence of sodium borohydride. Due to its high solubility, $GaCl_3$ [40] was used to synthesise Ga-LTf instead of $GaNO_3$, which reacts with reducing agents and produces heat which may denature the protein, LTf, before complexation. As shown from FTIR, all
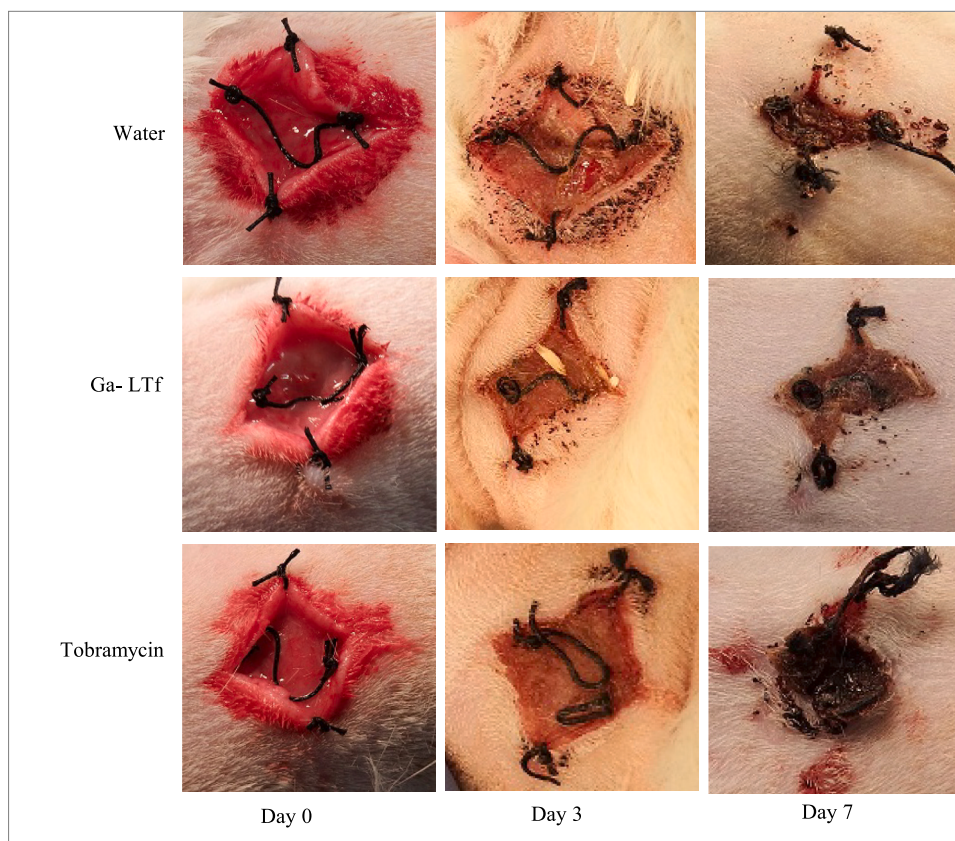
Fig. 4. Representative photographs taken at the beginning, 3rd day and 7th day of the *P. aeruginosa* infected wound after being treated with distilled water (negative control), Ga- LTf (experimental group) and tobramycin (positive control).

the functional groups of the pure LTf are present without any noticeable shifting of the major bands in Ga-LTf complex. This suggested that no chemical change occurs in the LTf during the complex formation reaction. The complexation experiments were performed in aqueous media to incorporate the Ga to LTf while avoiding any trace organic solvents or additives that might affect the complexation. The reducing agent sodium borohydride which is known to react with metals salts to form either free metal nanoparticles or its reduced form [41] was used. Being deliquescent and a soft Lewis acid with high polarizability, the $GaCl_3$ could react with water to form $Ga(OH)_2Cl$ and this in turn may form amorphous insoluble residues of HCl upon evaporation and will not favour the attempt to prepare Ga-LTf [Fig. 1 (a)]. In order to avoid the precipitation and residue formation, NaOH solution was used. Accordingly, NaCl but not HCl was produced as a reaction by-product. Furthermore, NaOH solution provided better reducing property to the protein and this could enhance the metal coordination [42].

As shown by ICP-OES, consistent local delivery of Ga^{3+} ions from the Ga-LTf complex makes it a unique Ga^{3+} delivery system unlike other reported gallium delivery agents [8,16,17,19] where the iron-binding complexes, such as transferrin and lactoferrin, could affect the local Ga^{3+} concentration. The use of Ga-LTf in this study achieved a statistically significant ($p < 0.04$) planktonic growth inhibition of *P. aeruginosa* compared with untreated samples. The inhibition of *P. aeruginosa* growth was directly proportional to the linear increase in Ga^{3+} ion release over time, the rate of Ga^{3+} ion release from Ga-LTf (0.6545 ppm/h). It is documented that iron release from hololactoferrin involves change in the conformation of the protein, carbonate loss and partial unfolding followed by protonation of the partially unfolded protein and requires specific interactions with the anions of the buffer [43]. LTf N-lobe contains the highest density of basic amino acids, which have been identified as the major binding sites to lactoferrin molecular targets [44]. Each lactoferrin molecule can reversibly bind two (Fe^{3+}) at the

binding sites, which are localized in each of the two protein globules and can bind a ferric ion (Fe^{3+}) together with a carbonate anion [45]. Although extrapolating structural conclusions from one metal to another is difficult, similarities in the coordination chemistry of Ga^{3+} with that of Fe^{3+} suggest that like Fe^{3+}, Ga^{3+} could be binding to LTf with each ion bonded with six ligands: four from the polypeptide chain (two tyrosine residues, one histidine residue and one aspartic acid residue) and two from carbonate or bicarbonate ions. Crystallographic studies on LTf have shown that the release of iron causes one domain to swing away from the other to open up the binding cleft [46]. Moreover, with K^+ and Na^+ the salt effect could be independent of the nature of the cation and occurs on two specific sites of Ga-LTf as reported for hololactoferrin [43]. The traces of sodium bromide found in the Ga-LTf complex prepared in this study potentially initiating protonation of the carbonate ion, tyrosine and histidine ligands, which weakens the binding to Ga^{3+} and leads to its release. However, characterisation techniques employed in this study to ascertain Ga-LTf complex formation and Ga^{3+} release are not sufficient to categorically establish potential mixture of any monogallium N-domain or monogallium C-domain or unspecific binding of Ga forms present in the Ga-LTf complex. Further analyses of Ga-LTF complex utilising ICP-OES, spectrophotometry and protein assays such as enzyme-linked immunosorbent assay (ELISA) may help to understand the proposed mechanism of gallium release from Ga-LTf involving ion exchanges. Alternatively, LTf cleft where Ga^{3+} is proposed to be binding first doesn't exert changes leading to the stable closed conformation and hence Ga^{3+} is easily replaced by more affinity ions. However, such a prediction needs to be explored with further analyses utilising techniques such as Small Angle Neutron Scattering and Neutron Spin Echo Spectroscopy.

However, bacteria such as *P. aeruginosa* have been known to grow as biofilms *in vivo* as an adaptive response to the adverse environment encountered during infection and extremely resistant to antibacterial
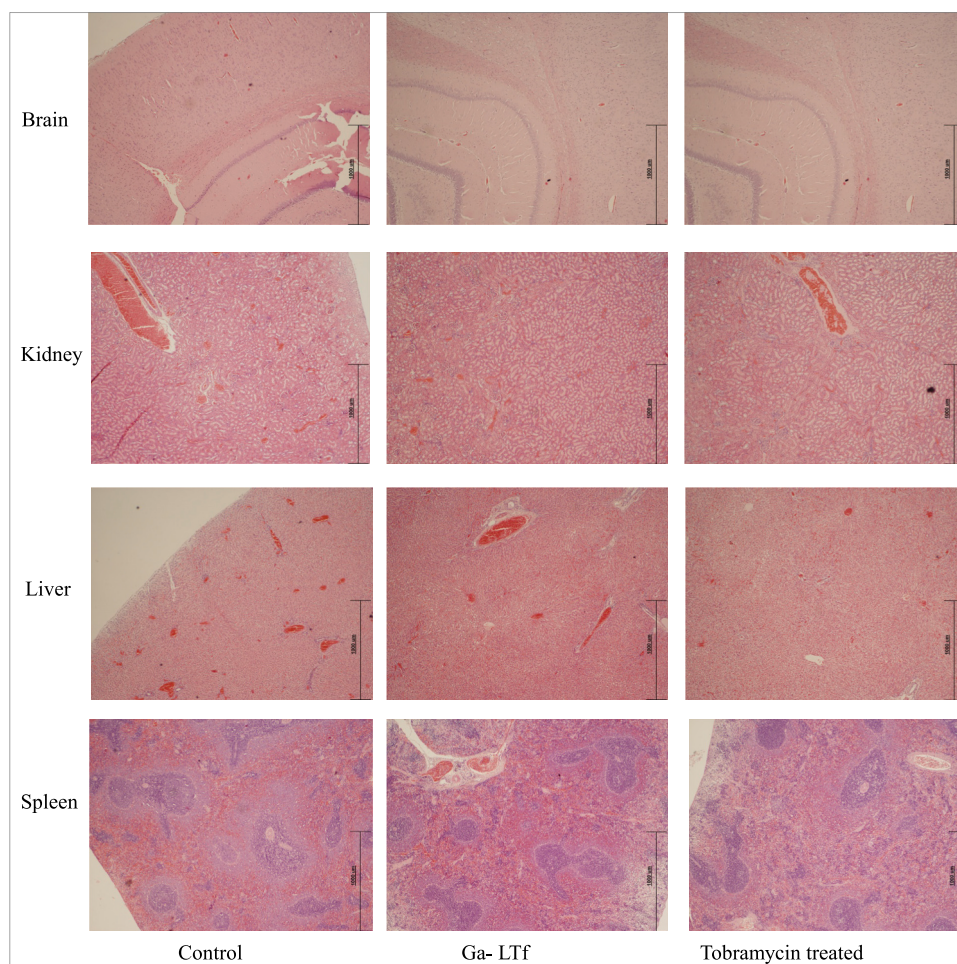
Fig. 5. Representative images of the brain, kidney, liver and spleen from control, Ga-LTf treated and tobramycin treated animals after day 7 in comparison to those treated with distilled water as negative control.

agents [3]. Bacteria embedded in biofilms exist in different metabolic states due to decreased oxygen and nutrient gradients from the surface to the bottom of the biofilm and are markedly different in their response to antimicrobials [3]. Notwithstanding the fact that biofilm architecture contains large water-filled channels that facilitate the free transport of solutes, the biofilm matrix displays a net negative charge due to the presence of DNA and anionic polysaccharides that can trap positively charged ions like Ga^{3+}. Thus, both the resting metabolic state of certain bacteria and the scavenging effect of the matrix could contribute to reducing the antimicrobial activity of Ga^{3+} in biofilm-growing bacteria if it is delivered through the currently reported methods agents [16,17,19]. However, delivering Ga^{3+} at target sites in the form of Ga-LTf will circumvent this scenario and help to maximise the exposure of *P. aeruginosa* growing as a biofilm to Ga^{3+}. If translated into clinical practice, higher Ga^{3+} dosages than those predictable from *in vitro* antimicrobial susceptibility testing on planktonic cells would be required for the successful therapy of biofilm-related infections [38]. Hence, further analyses of the Ga-LTf on *P. aeruginosa* biofilm grown in CDFF was conducted. The greatest antibiofilm effect of Ga-LTf on biofilm growth was observed at 24 h (2.24 $\log_{10}$ CFUs reduction). The result thus suggests that Ga-LTf may complement currently available antibacterial agents. These agents could offer some advantages over conventional therapeutic agents as antibiotic-resistant organisms; even those with multidrug resistance are likely to be sensitive to gallium [47]. This is probably due to the fact that gallium works by a fundamentally different mechanism to existing antimicrobial agents, as the Ga^{3+} has the potential to disrupt Fe^{3+} metabolism in a wide range of bacteria by Fe^{3+}

substitution [6]. However, the increase in CFUs counts seen for older biofilms indicates the need for longer exposure time of Ga-LTf to penetrate to the active cells growing within the core of the biofilm. *In vivo* studies conducted on Ga-LTf confirmed that the material is biocompatible at the tested concentration and it has a comparable effect to tobramycin in *P. aeruginosa* inoculated wound healing processes in the rat model.

P. aeruginosa employ siderophores such as pyoverdine (*Pvd*) [48] or pyochelin (*Pch*) [49] to transport Ga^{3+} into the bacteria where it could interfere with ribonucleotide reductase, mitochondrial function, and the regulation of transferrin receptor and ferritin [48,49]. Purified *Pvd* already reported to remove iron from 60 % and 100 % iron-saturated lactoferrin at physiological pH [50]. Moreover, variation of pH observed near chronic wound [51], particularly lower pH (pH 5) [52] could elevate siderophore production and Ga^{3+} uptake by *P. aeruginosa*. Furthermore, ability of Ga-LTf to bind bacterial lipopolysaccharide, found in Gram negative bacteria, through 18-loop region of the lacto-ferricin domain could be key in destabilizing bacterial membrane and increasing those bacterial permeability [53] and death. But consistent delivery of Ga^{3+} from Ga-LTf at the site of infection would be essential to maintain antibacterial effect and circumvent the iron scavenging mechanisms, such as excessive siderophore production or elastase secretion [54] or bacterioferritin-ferredoxin (BfrB-Bfd) complex [55] formation, employed by *P.aeruginosa*.

However, the fact that viable *P. aeruginosa* were not recovered in the wound washing experiments from any of the test animals, including the negative control, suggests that the bacterial load used to inflict the

wound infection was not a lethal dose. The method used to deliver *P. aeruginosa via* impregnation of the sutures is based on a previously published paper [30]. Modern sutures are often coated with wax to prevent them becoming brittle; this coating may have interfered with the delivery of *P. aeruginosa* and therefore the delivered amount of bacteria may not have been sufficient to create an infection. Considering the fact that animals have no underlying pathology, it might be difficult to create an overt infective wound. From this angle, the process of inducing infection with sutures that are dipped in *P. aeruginosa* solution should be revisited in a future study. Additionally, alternative methods *e.g.*, direct application of *P. aeruginosa* solution should be explored. Nonetheless, in order to overcome bioavailability in clinical application and to extend the action of Ga^{3+}, the use of Ga-LTf as topical gels to ensure high gallium concentrations at the site of infection could be an option. Versatility of this materials means it could also be useful in treating bacterial infections among diabetes patients who display abnormally high susceptibility to infection partly due to inactivation of endogenous lactoferrin.

5. Conclusion

The emergence of antibiotic resistance among pathogenic bacteria suggests an increasing demand for alternative strategies to combat such infections. The results from this study suggest that Ga-LTf may offer an effective alternative or complement to currently available antibacterial treatments, by allowing the controlled and local delivery of antibacterial gallium ions at infectious sites.

CRediT authorship contribution statement

Sabeel P. Valappil: Conceptualization, Funding acquisition, Methodology, Project administration, Supervision, Writing – original draft, Writing – review & editing. **Ensanya A. Abou Neel:** Formal analysis, Writing – original draft, Writing – review & editing. **Kazi M. Zakir Hossain:** Formal analysis, Investigation. **Willi Paul:** Formal analysis, Investigation, Project administration. **Durgadas Cherukaraveedu:** Formal analysis, Investigation. **Benjamin Wade:** Formal analysis, Investigation. **Tahera I. Ansari:** Formal analysis, Investigation. **Christopher K. Hope:** Supervision, Writing – review & editing. **Susan M. Higham:** Supervision, Writing – review & editing. **Chandra P. Sharma:** Funding acquisition, Project administration, Supervision, Writing – review & editing.

Declaration of competing interest

The authors declare that they have no known competing financial interests or personal relationships that could have appeared to influence the work reported in this paper.

Data availability

Data will be made available on request.

References

[1] T.I. Lin, Y.F. Huang, P.Y. Liu, et al., *Pseudomonas aeruginosa* infective endocarditis in patients who do not use intravenous drugs: analysis of risk factors and treatment outcomes, J. Microbiol. Immunol. Infect. 49 (2016) 516–522.

[2] V. Fabre, J. Amoah, S.E. Cosgrove, P.D. Tamma, Antibiotic therapy for *Pseudomonas aeruginosa* bloodstream infections: how long is long enough? Clin. Infect. Dis. 69 (2019) 2011–2014.

[3] F. Minandri, C. Bonchi, E. Frangipani, F. Imperi, P. Visca, Promises and failures of gallium as an antibacterial agent, Future Microbiol. 9 (2014) 379–397.

[4] Z. Pang, R. Raudonis, B.R. Glick, T.-J. Lin, Z. Cheng, Antibiotic resistance in *Pseudomonas aeruginosa*: mechanisms and alternative therapeutic strategies, Biotechnol. Adv. 37 (2019) 177–192.

[5] A.T. Nguyen, M.J. O'Neill, A.M. Watts, et al., Adaptation of iron homeostasis pathways by a *Pseudomonas aeruginosa* pyoverdine mutant in the cystic fibrosis lung, J. Bacteriol. 196 (2014) 2265–2276.

[6] Y. Kaneko, M. Thoendel, O. Olakanmi, B.E. Britigan, P.K. Singh, The transition metal gallium disrupts *Pseudomonas aeruginosa* iron metabolism and has antimicrobial and antibiofilm activity, J. Clin. Invest. 117 (2007) 877–888.

[7] S.P. Valappil, G.J. Owens, E.J. Miles, et al., Effect of gallium on growth of *Streptococcus mutans* NCTC 10449 and dental tissues, Caries Res. 48 (2014) 137–146.

[8] S.P. Valappil, D. Ready, E.A. Abou Neel, et al., Controlled delivery of antimicrobial gallium ions from phosphate-based glasses, Acta Biomater. 5 (2009) 1198–1210.

[9] C.D. Nadell, K. Drescher, N.S. Wingreen, B.L. Bassler, Extracellular matrix structure governs invasion resistance in bacterial biofilms, ISME J. 9 (2015) 1700–1709.

[10] T.B. Rasmussen, M. Givskov, Quorum-sensing inhibitors as anti-pathogenic drugs, Int. J. Med. Microbiol. 296 (2006) 149–161.

[11] E. Oh, K.J. Andrews, B. Jeon, Enhanced biofilm formation by ferrous and ferric iron through oxidative stress in *campylobacter jejuni*, Front. Microbiol. 9 (2018) 1204.

[12] B. Leyland-Jones, Treating cancer-related hypercalcemia with gallium nitrate, J. Support. Oncol. 2 (2004) 509–516.

[13] L.R. Bernstein, Mechanisms of therapeutic activity for gallium, Pharmacol. Rev. 50 (1998) 665–682.

[14] K.J. Logan, P.K. Ng, C.J. Turner, et al., Comparative pharmacokinetics of ^{67}Ga and ^{59}Fe in humans, Int. J. Nucl. Med. Biol. 8 (1981) 271–276.

[15] C. Bonchi, F. Imperi, F. Minandri, P. Visca, E. Frangipani, Repurposing of gallium-based drugs for antibacterial therapy, Biofactors 40 (2014) 303–312.

[16] L.R. Bernstein, L. Zhang, Gallium maltolate has in vitro antiviral activity against SARS-CoV-2 and is a potential treatment for COVID-19, Antivir. Chem. Chemother. 28 (2020), 2040206620983780.

[17] E. Banin, A. Lozinski, K.M. Brady, et al., The potential of desferrioxamine-gallium as an anti-*Pseudomonas* therapeutic agent, Proc. Natl. Acad. Sci. U. S. A. 105 (2008) 16761–16766.

[18] Z. Xu, X. Zhao, X. Chen, Z. Chen, Z. Xia, Antimicrobial effect of gallium nitrate against bacteria encountered in burn wound infections, RSC Advances 7 (2017) 52266–52273.

[19] S.P. Valappil, H.H.P. Yiu, L. Bouffier, et al., Effect of novel antibacterial gallium-carboxymethyl cellulose on *Pseudomonas aeruginosa*, Dalton Trans. 42 (2013) 1778–1786.

[20] M.G. Best, C. Cunha-Reis, A.Y. Ganin, et al., Antimicrobial properties of gallium (III)- and Iron(III)-loaded polysaccharides affecting the growth of *Escherichia coli, Staphylococcus aureus* and *Pseudomonas aeruginosa, in vitro*, ACS Appl. Bio Mater. 3 (2020) 7589–7597.

[21] G. Ramesh, J.E. Kaviyil, W. Paul, R. Sasi, R. Joseph, Gallium-curcumin nanoparticle conjugates as an antibacterial agent against *Pseudomonas aeruginosa*: synthesis and characterization, ACS Omega. 7 (2022) 6795–6809.

[22] P.F. Levay, M. Viljoen, Lactoferrin: a general review, Haematologica 80 (1995) 252–267.

[23] P.L. Masson, J.F. Heremans, C.H. Dive, An iron-binding protein common to many external secretions, Clin. Chim. Acta 14 (1966) 735–739.

[24] J.K. Actor, S.-A. Hwang, M.L. Kruzel, Lactoferrin as a natural immune modulator, Curr. Pharm. Des. 15 (2009) 1956–1973.

[25] M.E. Drago-Serrano, R. Campos-Rodríguez, J.C. Carrero, M. de la Garza, Lactoferrin: balancing ups and downs of inflammation due to microbial infections, Int. J. Mol. Sci. 18 (2017) 501.

[26] S.H. Wong, N. Francis, H. Chahal, et al., Lactoferrin is a survival factor for neutrophils in rheumatoid synovial fluid, Rheumatology (Oxford) 48 (2009) 39–44.

[27] M.L. Kruzel, M. Zimecki, J.K. Actor, Lactoferrin in a context of inflammation-induced pathology, Front. Immunol. 8 (2017) 1438.

[28] J.M. Andrews, BSAC Working Party on Susceptibility Testing. BSAC standardized disc susceptibility testing method (version 4), J. Antimicrob. Chemother. 56 (2005) 60–76.

[29] S.P. Valappil, E.A. Abou Neel, D.M. Pickup, et al., Antibacterial, remineralising and matrix metalloproteinase inhibiting scandium-doped phosphate glasses for treatment of dental caries, Dent. Mater. 38 (2022) 94–107.

[30] R.J. McRipley, R.R. Whitney, Characterization and quantitation of experimental surgical-wound infections used to evaluate topical antibacterial agents, Antimicrob. Agents Chemother. 10 (1976) 38–44.

[31] D. Legrand, Overview of Lactoferrin as a natural immune modulator, J. Pediatr. 173 (2016) S10–S15.

[32] A. Håkansson, B. Zhivotovsky, S. Orrenius, H. Sabharwal, C. Svanborg, Apoptosis induced by a human milk protein, Proc. Natl. Acad. Sci. U. S. A. 92 (1995) 8064–8068.

[33] J. Almowalad, S. Somani, P. Laskar, et al., Lactoferrin-bearing gold nanocages for gene delivery in prostate cancer cells *in vitro*, Int. J. Nanomedicine 16 (2021) 4391–4407.

[34] G. Duca, L. Anghel, R.V. Erhan, Structural aspects of lactoferrin and serum transferrin observed by FTIR spectroscopy, Chem J. Moldova. 13 (2018) 111–116.

[35] Y. Yuan, C. Brady, L. Annamalai, R.F. Lobo, B. Xu, Ga speciation in Ga/H-ZSM-5 by in-situ transmission FTIR spectroscopy, J. Catal. 393 (2021) 60–69.

[36] T.T. Le, C. Pistidda, J. Puszkiel, et al., Efficient synthesis of alkali borohydrides from mechanochemical reduction of borates using magnesium–aluminum-based waste, Metals 9 (2019) 1061.

[37] J. Mao, Q. Gu, Z. Guo, H.K. Liu, Sodium borohydride hydrazinates: synthesis, crystal structures, and thermal decomposition behavior, J. Mater. Chem. A 3 (2015) 11269–11276.

[38] W.R. Harris, V.L. Pecoraro, Thermodynamic binding constants for gallium transferrin, Biochemistry 22 (1983) 292–299.

[39] C. Conesa, L. Sánchez, M.D. Pérez, M. Calvo, A calorimetric study of thermal denaturation of recombinant human lactoferrin from rice, J. Agric. Food Chem. 55 (2007) 4848–4853.

[40] S. Avivi, Y. Mastai, G. Hodes, A. Gedanken, Sonochemical hydrolysis of Ga^{3+} ions: synthesis of scroll-like cylindrical nanoparticles of gallium oxide hydroxide, J Amer Chem Soc. 121 (1999) 4196–4199.

[41] G.N. Glavee, K.J. Klabunde, C.M. Sorensen, G.C. Hadjapanayis, Borohydride reductions of metal ions. A new understanding of the chemistry leading to nanoscale particles of metals, borides, and metal borates, Langmuir 8 (1992) 771–773.

[42] T. Sato, H. Oishi, Solvent extraction of gallium(III) from sodium hydroxide solution by alkylated hydroxyquinoline, Hydrometallurgy 16 (1986) 315–324.

[43] F. Bou-Abdallah, J.M. ElHage Chahine, Transferrins., Iron release from lactoferrin, J. Mol. Biol. 303 (2000) 255–266.

[44] B. Andersen, H. Baker, G. Morris, et al., Apolactoferrin structure demonstrates ligand-induced conformational change in transferrins, Nature 344 (1990) 784–787.

[45] L. Rosa, A. Cutone, M.S. Lepanto, R. Paesano, P. Valenti, Lactoferrin: A natural glycoprotein involved in iron and inflammatory homeostasis, Int J Mol Sci 15 (2017) 1985.

[46] B.F. Anderson, H.M. Baker, G.E. Norris, D.W. Rice, E.N. Baker, Structure of human lactoferrin: crystallographic structure analysis and refinement at 2.8 A^0 resolution, J. Mol. Biol. 209 (1989) 711–734.

[47] J.L. Graves Jr., A.J. Ewunkem, J. Ward, et al., Experimental evolution of gallium resistance in *Escherichia coli*, Evol Med Public Health 6 (2019) 169–180.

[48] G. Ghssein, Z. Ezzeddine, A review of *Pseudomonas aeruginosa* metallophores: Pyoverdine, Pyochelin and Pseudopaline, Biology 25 (2022) 1711.

[49] A. Braud, M. Hannauer, G.L. Mislin, I.J. Schalk, The *Pseudomonas aeruginosa* pyochelin-iron uptake pathway and its metal specificity, J Bacteriol. 191 (2009) 3517–3525.

[50] B.C. Jeong, C. Hawes, K.M. Bonthrone, L.E. Macaskie, Iron acquisition from transferrin and lactoferrin by *Pseudomonas aeruginosa* pyoverdin, Microbiol 143 (1997) 2497–2507.

[51] S. L., Percival McCarty, J.A. Hunt, E.J. Woods, The effects of pH on wound healing, biofilms, and antimicrobial efficacy, Wound Rep Regen. 22 (2014) 174–186.

[52] K. Harjai, R. Khandwaha, R. Mittal, V. Yadav, V. Gupta, S. Sharma, Effect of pH on production of virulence factors by biofilmcells of *Pseudomonas aeruginosa*, Folia Microbiol. 50 (2005) 99–102.

[53] M.E. Drago-Serrano, M. de la Garza-Amaya, J.S. Luna, R. Campos-Rodríguez, Lactoferrin-lipopolysaccharide (LPS) binding as key to antibacterial and antiendotoxic effects, Int. Immunopharmacol. 12 (2012) 1–9.

[54] G. Döring, M. Pfestorf, K. Botzenhart, M.A. Abdallah, Impact of proteases on iron uptake of *Pseudomonas aeruginosa* pyoverdin from transferrin and lactoferrin, Infect Immun. 56 (1988) 291–293.

[55] S. Anabel, H. Yao, J.R. Chandler, M. Rivera, Inhibiting iron mobilization from bacterioferritin in *Pseudomonas aeruginosa* impairs biofilm formation irrespective of environmental iron availability, ACS Inf Dis. 6 (2020) 447–458.